Tailoring the hydrophobicity of wrinkled silica nanoparticles and of the adsorption medium as a strategy for immobilizing lipase: An efficient catalyst for biofuel production

Giulio Pota [a,1], Aurelio Bifulco [a,1], Dambarudhar Parida [b], Shanyu Zhao [c], Daniel Rentsch [d], Eugenio Amendola [e], Valeria Califano [f,*], Aniello Costantini [a,**]

[a] *Department of Chemical, Materials and Production Engineering, University of Naples Federico II, Piazzale Tecchio 80, 80125, Fuorigrotta, Naples, Italy*

[b] *Laboratory for Advanced Fibers, Swiss Federal Laboratories for Materials Science and Technology (Empa), Lerchenfeldstrasse 5, 9014, St. Gallen, Switzerland*

[c] *Laboratory for Building Energy Materials and Components, Empa, Swiss Federal Laboratories for Materials Science and Technology, Überlandstrasse129, Dübendorf, CH-8600, Switzerland*

[d] *Laboratory for Functional Polymers, Swiss Federal Laboratories for Materials Science and Technology (Empa), 8600, Dübendorf, Switzerland*

[e] *Institute for Polymer, Composites and Biomaterials (IPCB), National Research Council of Italy (CNR), Piazzale Enrico Fermi 1, 80055, Portici, Naples, Italy*

[f] *Institute of Science and Technology for Sustainable Energy and Mobility (STEMS), National Research Council of Italy (CNR), Viale Marconi 4, 80125, Naples, Italy*

* Corresponding author.

** Corresponding author.

E-mail addresses: valeria.califano@stems.cnr.it (V. Califano), anicosta@unina.it (A. Costantini).

1 These authors equally contributed to the work.

Keywords:
Hydrophobic silica nanoparticles Lipase adsorption
Biodiesel
Interfacial activation

ABSTRACT

Hydrophobic wrinkled silica nanoparticles (WSNs) were obtained by surface functionalization with per- fluorodecyltriethoxysilane (PDTES) by chemical vapour deposition (CVD). Surface functionalization was made to design a hydrophobic surface to immobilize lipase in its open active conformation by interfacial activation. Moreover, to modulate the closed/open form equilibrium, favouring the open conformation, n-hexane was added to the water/lipase solution, creating a micro-oily environment. Physicochemical characterization of supports was carried out by solid state ^{29}Si nuclear Magnetic Resonance (NMR), the Brunauer–Emmett–Teller (BET) method, thermogravimetric (TG) analysis, contact angle (CA) measurement, scanning electron microscopy (SEM) and Fourier transform infrared (FT-IR) spectroscopy. Three different supports for physical immobilization of lipase were prepared, differing in the degree of hydrophobicity. The effect of the different hydrophobicity and of the addition of n-hexane on the adsorption of lipase was evaluated. The hyperactivation of the best biocatalyst was tested in the hydrolysis and transesterification of sunflower seed oil and compared to free lipase. The re- action yields were 87% and 75% respectively for hydrolysis, and 93% and 56% respectively for trans- esterification. The results suggest that both the hydrophobicity of the support and the addition of n-hexane favour the adsorption of lipase in the active conformation.

1. Introduction

Rapid depletion of fossil fuel sources, together with the increasing impact of greenhouse-gas emissions on climate changes, triggered the search for carbon-neutral biofuels. Biodiesel, consisting of fatty acid alkyl esters, stands as a renewable fuel that has received growing attention in last decades for its use for automotive application [1]. Biodiesel is produced by transesterification of triacylglycerols, a widely available substrate contained in vegetable oils. Transesterification re- action can be catalyzed by lipases (E.C. 3.1.1.3). Lipases are extracted from different sources. They are involved in several biochemical re- actions on triacylglycerols, such as hydrolysis and esterifications. Literature is rich of papers dealing with the lipase-catalyzed biocon- version of oils into biodiesel [2–4]. High product purity, easy separation of the byproduct glycerol, lower energy consumption due to mild re- action conditions represent remarkable benefits deriving from the use of lipases in biodiesel production. Moreover, enzymatic transesterification leads to the complete conversion of free fatty acids (present in low-quality feedstock) to methyl/ethyl esters [5]. The yields of trans- esterification are usually affected by a series of factors such as lipase stability, specificity, reaction temperature and water content in the re- action medium [6,7]. In particular, lipases specificity can be a problem for biodiesel production, where the full conversion of the triglycerides is required [8].

Despite many benefits, the commercialization of the enzymatic bio- diesel is still hindered by the high cost and low stability of lipases. In order to make it competitive at the industrial level and reach a signifi- cant level of applications, it is necessary to overcome these drawbacks and improve recovery as well as recycling of the biocatalyst. To address these deficiencies, lipases can be immobilized on insoluble supports. Enzyme immobilization is the confinement of the enzyme molecules onto/within an insoluble support with retention of its catalytic activity. This methodology allows exploiting the advantages of heterogeneous catalysis. Furthermore, immobilization often results in the improvement of enzyme properties, such as stability, activity and selectivity [9,10], and decreases the effect of enzyme inhibitors (such as alcohols in case of lipase) and thermal inactivation [11]. Different techniques for enzyme immobilization can be used: adsorption, entrapment, covalent binding, and cross-linking [12].

A successful process of immobilization is expected to guarantee high activity and reusability for the immobilized enzyme, two key features strictly related to the physico-chemical properties of the chosen support [13]. Among all the nanostructured materials suitable for enzyme immobilization, mesoporous silica has recently gained attention as one of the most performing due to its endogenous properties such as low toxicity, high biocompatibility and good stability. High surface area, and tunable pore size and distribution allow high loading of guest species or pollutants [6,14–16]. Moreover, the abundant surface hydroxyl groups enable easy chemical surface functionalization [17–19].

Mesoporous silica nanoparticles (MSPs) with radial-oriented micro- channels and a conical pore shape are ideal scaffolds for catalytic ap- plications, as the pore structure is accessible to large molecules. This particular morphology allows enzyme molecules to diffuse smoothly into the pores promoting enzyme loading and minimizing diffusion limitations of reactants and products [20]. The positive outcome of these factors is

the enhancement of the catalytic performance of immobilized enzymes [21]. Wrinkled silica nanoparticles (WSNs) belong to this kind of nanoparticles [22]. They have radially widening pores that can easily host functional materials avoiding pore block. Several papers report the choice of WSNs as support for the immobilization of lipase [23] and β-glucosidase [24–26] so far. The improved catalytic performance exhibited by WSN-supported lipase compared to free enzyme was explained with the good dispersion of active sites inside the pores, due to the radially aligned mesopores of WSNs [23]. Similarly, an improvement of the catalytic performances, together with higher thermal and opera- tional stability, was obtained for WSN-supported β-glucosidase. Even then, this was attributed to the pore shape and the hierarchical pore structure which eliminate diffusive limitations for the substrate, making WSNs optimal hosts of β-glucosidase [24,25].

Generally, lipases immobilization requires the functionalization of the silica particles with hydrophobic moieties [27] and most lipases exhibit full catalytic activity only after interfacial activation. Lipases have a helical loop that covers their active site. In this "closed" conformation, the catalytic site is inaccessible and lipase is inactive. Upon adsorption at a hydrophobic/hydrophilic interface, the loop changes its conformation giving rise to the "open" active from Refs. [28–30]. Therefore, it is preferable to immobilize lipase in the open-lid active conformation [31]. This is possible by using hydrophobic sup- ports. Lipase undergoes interfacial activation during immobilization on hydrophobic support similarly similarly to what happens when lipase is at the interface with its natural substrate [32,33]. Furthermore, due to the mechanism of interfacial activation, lipases tend to form dimers in aqueous solution through the interaction of the active centres of two molecules in the open form, which are in equilibrium with the monomer [33,34]. The dimeric form is less active than the monomeric one and immobilization on hydrophobic supports causes a shift of the dimer/monomer equilibrium of the lipase towards the monomer form, which is readily adsorbed in the open form. For these reasons, lipase activity sensibly improves when the protein is immobilized on hydro- phobic supports [33–35]. For biodiesel production, the use of hydro- phobic support is also favourable because the accumulation of hydrophilic compounds during the transesterification reaction, i.e. glycerol or water, can lead to enzyme deactivation. Glycerol can hinder the lipase activity by creating a hydrophilic shell around the enzyme that prevents the hydrophobic substrate to diffuse to the active site [36]. This effect can be reduced in several ways, for example by using ultra- sounds [37], molecular sieves [38] or hydrophobic supports [39,40].

In this work, *Candida rugosa* lipase (CRL) was physically immobilized onto hydrophobic functionalized WSNs to preserve its native confor- mation and catalytic activity. Immobilization was carried out using a ternary system lipase/water/n-hexane (a micro-oily environment). This was possible because it was found that a 0.2% wt. solution of lipase in water can solubilize small quantities of the oil phase forming a clear solution [41]. The addition of n-hexane was made to modulate the equilibrium between the open and the closed form of lipase. In fact, it was found that some water insoluble organic solvent (i.e. hexane) can induce the opening of the lid increasing lipase activity [42]. Lipase adsorption on hydrophobic supports is enhanced when the open form of the lipase is favoured in solution. For example, using octyl agarose as support, it was found that the lipase immobilization rate increased when the ionic strength decreased [31,43]. At high ionic strength, the closed form is favoured because the open form exposes a large hydrophobic pocket, and lipase/lipase dimers are stabilized. That is, the closing/op- ening equilibrium of lipase can be modulated by altering the adsorption medium and the adsorption rate on hydrophobic surfaces increases when the equilibrium is shifted towards the open form. Similar results have been obtained which show how the composition of the lipase adsorption medium on hydrophobic supports alters its properties, probably for its structural flexibility due to the presence of the lid [44]. In fact, it was found that immobilization of lipases with small lids, un- able to fully isolate the active center to the medium, is not influenced by the medium composition, unlike to what happen with the immobiliza- tion of lipases with larger lids [45]. Despite hexane may compete with the surface of the support in the adsorption process, it must be consid- ered that lipases generally have a high character of hydrophobicity, especially when they are in open form, as shown in Fig. 1. When the lid is open, a large hydrophobic surface is exposed around the catalytic tun- nel, so that the interaction with the solid surface is still possible even if the active site is interacting with hexane. The adsorption on the solid surface stiffens the lipase structure so that this conformational state is maintained after immobilization on hydrophobic supports.

The WSNs surface was modified using perfluorodecyltriethoxysilane (PDTES) as the hydrophobic agent. We have prepared three kinds of samples using a different amount of PDTES, which have shown adifferent level of hydrophobicity. The enzyme derivatives were used both for triglyceride hydrolysis and transesterification reactions.

2. Experimental

2.1. Materials

Tetraethyl orthosilicate (TEOS), cetyltrimethylammonium bromide (CTAB), urea, cyclohexane, isopropanol, ethanol (ACS reagent, anhy- drous), hydrochloric acid (37 wt% in water), distilled water, per- fluorodecyltriethoxysilane (PDTES), lipase from *Candida Rugosa*, n- hexane, and Span® 80 were bought from Sigma-Aldrich (Milan) and used as purchased. Sunflower oil high-oleic (SOHO) (density 0.92 g/cm^3, 786 g/mol average molecular weight [46]) was purchased from a local supermarket.

2.2. Synthesis and surface hydrophobization of wrinkled silica nanoparticles

Wrinkled Silica Nanoparticles (WSNs) were synthesized as previ- ously described [25] and following the procedure described by Moon and Lee [22] with slight modifications. More specifically, CTAB was used as the surfactant instead of cetylpyridinium bromide (CPB) and a more accurate surfactant removal procedure was carried out.

Hydrophobic WSNs were produced by chemical vapour deposition (CVD), as described in Fig. 2. 50 mg of WSNs were homogeneously settled on a Petri dish by drop casting of a WSNs-ethanol dispersion. After the evaporation of the solvent, the dried nanoparticle surface un- derwent CVD process. The Petri dish was placed on a heating plate at the temperature of 100 °C. 5 mL of PDTES-ethanol solution was settled dropwise close to the external borders of the Petri dish. The whole system was rapidly covered by a ceramic dome with an exhaust beak, allowing the hydrophobic solution to evaporate completely. To obtain WSNs with different hydrophobicity behaviours, 1%, 5% and 10% by volume of PDTES in ethanol solution were used. Three samples were named **WSN1**, **WSN5**, and **WSN10**, where the percentage in the acro- nyms refers to the volume concentration of PDTES-in-ethanol solutions used during the CVD process. PDTES/WSN weight ratio was set to 1.7, 8.5, and 17 for **WSN1**, **WSN5**, **WSN10**, respectively. Finally, silanized nanoparticles were scratched off the Petri dish and ground to obtain a fine powder that was subsequently used for physical immobilization.

2.3. Preparation of hydrophobic coated surfaces

To evaluate the hydrophobic properties of functionalized WSNs, a set of coated glass slides was prepared to perform surface wettability measurements. Briefly, 12 mm diameter circular glass slides were hydrophilized by oxygen plasma etching (2 min at 0.5 mbar) to activate glass silanol groups. The activation of the glass surface is needed to lower the water contact angle and improve the affinity with WSN water dispersion. 150 μL of 67 mg/mL WSNs aqueous suspension was placed dropwise on the surface of the supports to have a coating of 8.85 mg/ cm^2. Finally, the glass slides were dried in a aerated oven at 100 °C for 20 min, obtaining dried supports with 10 mg of nanoparticles that homogenously covered the surface of each support. WSN-coated supports were submitted to CVD using the same experimental apparatus reported above. In this case, 1 mL of PDTES-in-ethanol solution was used. 1%, 5%, and 10% in volume of PDTES in ethanol solutions were used for hydrophobization and the coated surfaces were named as the nanoparticles settled onto them (**WSN1**, **WSN5**, and **WSN10**, respectively).

2.4. Physical-chemical characterization

2.4.1. Scanning electron microscopy (SEM)

A FEI Nova NanoSEM 230 (FEI, Hillsboro, Oregon, USA) was used to collect Scanning Electron Microscopy (SEM) images, at an accelerating voltage of 10 kV. A WSN suspension in ethanol was ultra-sonicated for 10 min, settled on an aluminum support of 70 μm in thickness and dried at room temperature. Before the analysis, the samples were coated with a Platinum layer of about 10 nm, which corresponds to the thickness of the platinum coating on the quartz sensor.

2.4.2. N_2 physisorption

Bare and functionalized WSNs were submitted to N_2 adsorption/ desorption analysis to determine the specific surface area and the pore structure. The samples were degassed for 10 h at 0.03 mbar and 100 °C. Afterwards, a Micromeritics TriFlex instrument was used to collect N_2 adsorption/desorption isotherms with 10-s equilibration time. Bru- nauer–Emmett–Teller (BET) method was chosen to calculate the specific surface area, whereas the application of Barrett–Joyner–Halender (BJH) model on the adsorption branch of the isotherm provided the pore size distributions and pore diameter.

2.4.3. Measurement of surface wettability

A Dataphysics OCA 30 instrument was exploited to detect the wettability, the contact angle (CA), the roll-off angle and the contact angle hysteresis (CAH) of nanoparticles. In particular, as concerns the contact angles as well as the roll-off angles of distilled water were both measured at around 21 °C. To estimate the contact angle hysteresis, the titlted plane methodology was adoperated and CAH was measured as the contact angle that a droplet of distilled water shows when is posed on an inclined plane and starts descending [47]. In detail, the tilting of the solid sufaced leads to the deformation of the droplet and thus the contact angle hysteresis was calculated as the difference between the advancing and the receding contact angles. The contact angle was also estimated in case of diiodomethane. The data of weattability collected by using diiodomethane and water were subsequently deployed to determine the surface free energy of hydrophobic solid surfaces through the Owens, Wendt, Rabel, and Kaelble (OWRK) method [48]. In particular, all the CAs were evaluated by posing liquid droplets with a valume ranging from 6 to 9 μl on the surface.

2.4.4. Thermogravimetric (TGA) analysis

TGA analysis of WSN samples was carried out to assess the degree of functionalization and efficiency of silanization as well as the amount of enzyme loaded onto the nanoparticles. 10 mg of sample was analysed in a TA Instrument simultaneous thermoanalyser SDT Q600 within the temperature range of 25 °C–1000 °C with a heating rate of 10 °C/min. The organic content in bare WSNs and functionalized WSNs was eval- uated following equation (1), where W_1 and W_2 are the sample weight at 200 °C and 1000 °C respectively.

$$\textbf{Organic content}\ (\%) = \frac{W1 - W2}{W1} \times 100 \qquad \text{(eq. 1)}$$

2.5. Lipase immobilization onto WSN

The whole procedure from WSNs hydrophobization to lipase adsorption is schematically shown in Fig. 2. Lipase was physically immobilized onto bare WSNs and hydrophobic WSNs from a ternary oil- water-enzyme medium and a binary water-enzyme solution (the latter only for sample **WSN5**). In detail, 25 mg of the enzyme were dissolved in 25 mL of distilled water under magnetic stirring for 30 min. 200 μL of n- hexane was added dropwise to the water-enzyme solution. No phase separation was observed after the addition of hexane. Subsequently, 50 mg of nanoparticles were added to the adsorption mixture and then diluted with 12.5 mL distilled water to improve the nanoparticle dispersion. The system was kept under stirring for 24 h as previously determined by Califano et al. to immobilize β-glucosidase enzyme on WSNs [25,50]. The supported biocatalysts were recovered by centrifu- gation and washed twice with distilled water to remove the non-adsorbed enzymes. The samples obtained after lipase immobiliza- tion were named **L-WSN**, **L-WSN1**, **L-WSN5**, **L-WSN10** based on the type of wrinkled silica supports used **L-WSN5-w** was immobilized in distilled water without the addition of n-hexane. The enzyme immobi- lization in each sample was determined by TGA analysis by subtracting the organic content of each support from the one of the corresponding biocatalysts. The yield of immobilization (YI %) was calculated as the weight ratio between the adsorbed enzyme and the amount dissolved in the adsorption mixture. The enzyme conformation on the nanoparticle surface was investigated by FTIR spectroscopy.

2.6. Catalytic assay

2.6.1. Hydrolysis of sunflower seed oil

Free and supported lipase were tested for room temperature hydro- lysis of triglycerides into free fatty acids and glycerol. Typically, 500 μL of Span® 80 was mixed with 10 mL of SOHO sunflower oil (source of vegetable triglycerides) in a 25 mL conic flask. For the free enzyme, 2 mL of a lipase aqueous solution of three different concentrations, 0.4, 0.56, and 0.8 mg/mL were added dropwise to the mixture under stirring to obtain a

white water-in-oil emulsion. The amount of water was chosen to ensure an oil-to-water 1:10 M ratio. After 48 h, the reaction mixture

Fourier-transform infrared (FTIR) spectroscopy

Fourier transform infrared (FT-IR) spectroscopy was performed with a Nexus FT-IR spectrometer equipped with a DTGS KBr (deuterated triglycine sulfate with potassium bromide windows) detector. Samples were prepared by pelleting in KBr and the spectra were recorded in the range 4000 - 400 cm^{-1} at a spectral resolution of 2 cm^{-1}. The spectrum of each sample was corrected by subtracting of the spectrum of blank KBr.

Curve fitting of the amide I band of **L-WSN5** and **LWSN5-w** was performed by GRAMS/32 (Galactic Industries Corporation, Salem, NH, U.S.A.) as a linear combination of Gaussian components. The number and position of components were taken from the second derivative spectrum. Second derivative spectra were obtained following the Savitsky–Golay method (3rd-grade polynomial, five points of smooth- ing). Initial values of bandwidths and intensities were automatically generated.

2.4.5. ^{29}Si nuclear Magnetic Resonance

The cross-polarization (CP) magic-angle spinning (MAS) NMR spectra of starting material **WSNs** and functionalized WSNs (**WSN10**) were recorded using a 7 mm CP MAS probe on a Bruker Avance III 400 NMR spectrometer equipped with a wide-bore 9.4 T magnet, corre- sponding to 1H and ^{29}Si Larmor frequencies of 400.2 and 79.5 MHz, respectively. A detailed description of the procedure can be found in the experimental section of the work by Stojanovic et al. [49].

was transferred to a separating funnel and 50 mL of n-hexane was added to it for extraction of glycerol (bottom) and oil phase (top). Finally, the resulting glycerol was recovered by centrifugation and dried overnight in an oven at 80 °C. The yield of the reaction (YR%) was determined as per equation (2). Where, $n_{glycerol}$ and $n_{triglycerides}$ refer to the moles of product and substrate, respectively.

$$\mathbf{YR(\%)= (n_{glycerol}/n_{triglycerides})\cdot 100} \quad (2)$$

For the immobilized enzyme, only 0.56 mg/mL lipase concentration was tested. Prior to the extraction of glycerol, the biocatalyst was recovered by centrifugation. The chemical nature of the reaction prod- uct (e.g. glycerol) was evaluated through FTIR spectroscopy in the attenuated total reflection (ATR) mode by using DuraSam-plIR II accessory equipped with ZnSe Crystal.

2.6.2. Operational stability

The immobilized biocatalyst was subjected to seven consecutive catalytic cycles (each 48h) for evaluation of its reusability. Each reaction was carried out under standard assay conditions. After each cycle, the solution was centrifuged to recover the catalyst and the supernatant underwent the same experimental route to determine the amount of glycerol produced. The yield after the first cycle of the reaction was used as the reference (e.g. 100% conversion).

2.6.3. Transesterification of sunflower seed oil

Free and supported lipase were tested as biocatalyst for the trans- esterification between ethanol and SOHO sunflower seed oil into esters of fatty acids and glycerol. For both free and immobilized lipase, the enzyme concentration was maintained at 0.56 mg/mL 9.2 g (10 mL) of sunflower seed oil were mixed with 500 μL of Span80 surfactant and 2 mL of ethanol was used for the reaction. To minimize ethanol inhibition of lipase, the ethanol addition was partitioned in a three-step batch ethanolysis. In particular, a third of the overall ethanol volume (about 700 μL) was added dropwise to the oil-surfactant mixture under stirring. Subsequently, the chosen amount of enzyme was dispersed into the re- action mixture. The remaining ethanol volume was added in two equal aliquots after three and 6 h, respectively. The reaction was carried out for 48h at room temperature. The yield of the reaction was determined as previously reported for the hydrolysis reaction.

3. Results and discussion

Considering the high available surface area and easy dispersibility wrinkled silica nanoparticles were considered as the support and were synthesized by the method reported earlier [19]. However, it is well known that immobilization of lipase is favoured by the hydrophobicity of the surface [31]. Therefore, WSNs were functionalized by CVD using PDTES as a precursor. To evaluate the effect of functionalization on properties of WSNs, different concentration (1, 5 and 10%) of PDTES was used during CVD.

3.1. Scanning electron microscopy (SEM) analysis

Analysis of pristine WSN sample under SEM revealed the formation of spherical nanoparticles with a highly porous structure (Fig. 3a). The average diameter of WSNs was found to be 300 nm with a uniform distribution. No dimensional and geometric differences are noted be- tween the samples **WSN**, **WSN1**, and **WSN5** (Fig. 3a–c). However, in the case of **WSN10**, the presence of small pseudospheric clusters was observed (Fig. 3d).

3.2. Hydrophobic properties of functionalized WSNs

As a measure of successful functionalization, contact angle (CA), contact angle hysteresis (CAH), and roll-off angle were measured after uniformly depositing WSNs on a circular glass slide of 12 mm in diam- eter. According to the CA (θ), a surface can be classified as super hy- drophilic when $\theta \approx 0^{\circ}$ (using water as the liquid). When, $\theta < 90^{\circ}$ the surface is hydrophilic and surface is hydrophobic at $\theta > 90^{\circ}$ [51,52]. CA of functionalized WSNs indicate their excellent hydrophobicity (Fig. 3e). In particular, both **WSN5** and **WSN10** can be considered as super-hydrophobic (Fig. 3e and Table S1). Notably, CAH and roll-off angles attain very low values (Table S1), which explains the hierarchi- cal surface texture formed due to the nanometric roughness present on the surface of the WSNs. The hydrophobicity obtained during this study (Table S1) highlights the efficiency of the CVD treatment.

The surface free energy (SFE) of WSNs was also measured to elimi- nate the effect of liquids used for measurement on CA. The determina- tion of SFE in necessary to achieve a complete comprehension of the wettability properties of surfaces. In particular, the Owens, Wendt, Rabel, and Kaelble (OWRK) model equation can be applied for the estimation of SFE and its components (e.g. dispersive and polar) [51, 53–55]. The values of SFE were evaluated by the OWRK method and are listed in Table S2. The values of these three parameters obtained in the case of

functionalized WSNs are much lower than the reported values obtained following the same procedure [56,57]. A low affinity with polar substances results in low values for the polar term of surface free energy, which is beneficial since lipase adsorption is boosted by hy- drophobic surfaces as functionalized WSN. A high degree of hydropho- bicity after functionalization of WSN (e.g. **WSN1**, **WSN5**, and **WSN10**) makes these supports suitable for lipase immobilization via interfacial adsorption, because of the well-known interaction between the open conformation of the enzyme with hydrophobic surfaces. It is reported that the immobilization of lipases on hydrophobic matrices with extended porous structure usually results in an enhancement of the ac- tivity of lipases [34,39,58]. Adsorption is based on physical interactions between the enzyme and the silica nanostructure, such as van der Waals forces, and ionic interactions.

3.3. N_2 adsorption-desorption measurements

The specific surface area of the synthesized WSNs was calculated from the low-pressure range (0.07–0.30 of p/p_0) of the N_2 sorption isotherm (Fig. 4a). The pore size distribution was evaluated from the adsorption part of the isotherm (Fig. 4b). The adsorption-desorption isotherm shows the WSN samples have type IV pore structure with a small H3 hysteresis starting from $p/p_0 = 0.9$, which is ascribed to a presence of mesoporous structure with open ends slit shape [22], but from the BJH analysis (Fig. 4b), micropore is the dominated pore structure. The BET surface area and total pore volume of the four sam- ples are displayed in Fig. 4c. Fig. 4c shows a non-monotonous profile, with **WSN5** showing the maximum surface area and pore volume.

Fig. 4b shows that all samples have a narrow pore size distribution centred at 3.5 nm, and a broad peak around 10 nm corresponding to the average inter-wrinkles distance. The peak at 3.5 nm indicates that the wrinkles are mesoporous and the average inter-wrinkled distance de- creases from 10 nm to 8.5 nm going from the **WSN** sample to **WNS1**. However, further functionalization does not lead to any change in inter- wrinkle distance. This means that a part of the PDTES is deposited on the outer surface of the particles [59], and the deposition increases with increase in concentration of PDTES solution during CVD. Concentrations ≥1%, all the excess goes to the external surface. The anchoring of PDTES onto the surface of WSNs might be responsible of the enhancement of surface area as long as the space between the silane groups and the surface is sufficiently wide to adsorbe N_2 molecules [60]. Post synthetic functionalization of mesoporous silica mainly results in the modification of the outer particle surface and near the pore entrances since these sites are easily accessible [61]. This is the possible reason for the increase in the surface area up to a PDTES concentration of 5%. The decrease in the surface area of **WNS10** is due to the blocking of some pores, which is clearly visible in the SEM image (Fig. 3d). The hydrophobization process does not influence the size of the smallest pores, so it can be said that those pores remain empty.

3.4. NMR spectra of non-functionalized and functionalized WSN

The functionalization of WSNs with PDTES is shown in Fig. 5a. To confirm the reaction between siloxane groups of WSNs and PDTES solid-state ^{29}Si NMR analysis of pristine **WSNs** and **WSN10** was performed (Fig. 5b). For both samples, broad ^{29}Si MAS NMR resonances at -92, -101, and -110 ppm were attributed to the Q_2, Q_3, and Q_4 silica spe- cies, with the Q_2-and Q_3-groups localized at the surface [62]. While only the Q_n groups are visible in the **WSN** starting material, additional res- onances were observed at -58 and -67 ppm in the case of **WSN10**. They are assigned to the T_3 and T_2 groups, respectively, which originate from silica atoms in PDTES [63]. A barely visible shoulder at ~ -53 ppm could be due to a low proportion of T_1 groups. Successful grafting of PDTES to WSNs is accompanied by the increase in relative signal in- tensity of Q_4 and the simultaneous decrease of the Q_2 resonance (Fig. 5b). Both observations are consistent with the functionalization of WSNs with PDTES [63].

3.5. Lipase adsorption

A lipase adsorption experiment was carried out using water-lipase-n- hexane ternary system for all prepared WSN supports. For the **WSN5**, which is the most promising due to its highest surface area, adsorption was also carried out from a binary system consisting of lipase and water only. Lipase content, lipase loading per gram of support, and adsorption efficiency were determined from the TGA thermogram. The amount of enzyme adsorbed initially decreases (**WSN1**) due to the decrease in the average pore size, then increases to reach the maximum for **WSN5** (Fig. 6a). This can be attributed to the increase in the specific surface area and hydrophobicity. Adsorption from water alone on the **WSN5** support shows a lower uptake (68 vs. 80 mg/g of support) (Table S3). In the case of **WSN10**, a decrease in lipase adsorption can be due to blockage of pore entrance during functionalization, which can be seen in the SEM image of **WSN10** (Fig. 3d).

One of the main objectives of a well-designed immobilization process is to keep the secondary structure of the enzyme unaltered and to maintain the activity of lipase. It is worth mentioning here that during the immobilization, the enzyme can experience relevant changes in the conformation due to the interaction with the support or crowding effect, when enzyme molecules are forced into a small space [64]. To observe such conformational changes in lipase, FTIR spectroscopy was applied [65–67]. Quantitative information on the secondary-structure of the lipase was obtained by analysing the amide I absorption band in the range of 1600–1700 cm^{-1}. This band is generated by the C=O stretching vibration of the peptide group and is very sensitive to the molecular geometry, hydrogen bonding pattern, and dipole interactions along the secondary structures. The amide I band originates from the overlapping of several peaks associated to different structural elements such as α-helices, β-sheets, turns, and irregular structures. These secondary structures can be obtained by deconvolution of the amide I band into Gaussian components through curve fitting [68].

Fig. 6b shows the FTIR spectra (range of 1550–1850 cm^{-1}) of all samples with immobilized lipase on WSNs and lyophilized lipase. All adsorbed lipase from the ternary system lipase-water-hexane shows a shift of the amide I band toward lower wavenumber, possibly due to aggregation [41,69]. The shift is minimum in the case of **L-WSN5** (Fig. 6b). Lipase adsorbed from a water solution (**L-WSN5-w**) shows a shift of the amide I band toward higher wavenumbers. It can be assumed that in cases with only a small shift of the amide I band compared to the FT-IR spectrum of the native enzyme, a comparatively similar secondary structure of the bound enzyme should be present. FT-IR analysis pointed out that **L-WSN5** is the biocatalyst in which the secondary structure of the protein is best preserved and the amount of uptake lipase is the highest. **L-WSN5** and **L-WSN5-w** were then selected for subsequent studies. The amide I band fitting procedure described in the experimental section was applied to **L-WSN5** and **L-WSN5-w** spectra. Fig. 6c and d displays the experimental and calculated curves with best Gaussian fit components. The position and the assignment [70, 71] of the Gaussian components of the

amide I band are summarized in Table 1. The amount of the different secondary structures were estimated by the area underneath each Gaussian band/the total area of the peaks between 1600 and 1700 cm^{-1} (Table 2).

In both cases, except for a certain degree of aggregation, the secondary structure of the polypeptide seems quite preserved. A slight decrease of α-helix content and a slight increase in random-coil (unordered) structures in **L-WSN5-w** indicates a higher degree of unfolding compared to **L-WSN5**. On the other hand, hydrogen-bonded aggregates are ~~higherr~~ in the case of **L-WSN5**. The increase in the β-turn content in **L-WSN5-w** also indicates a change in the secondary structure [72].

3.6. Catalytic assays

Three different free lipase concentrations (0.40, 0.56, and 0.80 mg/ mL) were used for the hydrolysis of sunflower seed oil to evaluate the minimum amount of enzyme needed to achieve the maximum conver- sion at a fixed substrate concentration. To assess that triglycerides were converted after 48h, the ATR spectrum of the product was collected. The comparison with a reference spectrum confirmed that glycerol was produced [74]. 0.40 mg/mL concentration led to 56% conversion of the substrate after 48 h (Fig. 7a), while the yield of the reaction was enhanced to 76% by increasing the lipase concentration to 0.56 mg/mL. No significant improvement of the substrate conversion was detected with a further increase in the enzyme concentration to 0.80 mg/mL.

Thus, 0.56 mg/mL was identified as the enzyme amount needed to reach the regime conversion of 76%. This result led us to study the catalytic activity of supported catalysts keeping the lipase concentration in the reaction solution at 0.56 mg/mL. Only **L-WSN5** and **L-WSN5-w** were subjected to a catalytic reaction. Interestingly, **L-WSN5** achieved 87% conversion within 48 h. This is similar to what was reported in the literature for immobilized lipase for esterification of oleic acid with methanol [23]. Nevertheless, the transesterification of raw material, natural oils, is much more complex than the esterification of a simple fatty acid. The first difficulty originates from the heterogeneous chem- ical composition of natural oils [8]. Indeed, they are composed of tri- glycerides whose structure contains a number of fatty acids. Furthermore, since transesterification is a three-step reaction, signifi- cant conversion rates are achievable only if the enzymes exhibit activity also towards diglycerides and monoglycerides formed as reaction in- termediate [75].

The results of the hydrolysis highlight inactive-to-active conforma- tional changes of lipase when adsorbed at a hydrophobic/hydrophilic interface. Therefore, the physical interaction with silanized WSNs was found to be a successful method of immobilization and activation of lipase to achieve the high activity. This result is not surprising, since lipase immobilized on hydrophobized silica particles often showed hyperactivation [27,76,77]. However, **L-WSN5-w** was only able to achieve only 45% conversion at the same experimental condition. The lower hydrolytic activity is due to a change in the secondary structure of lipase during immobilization from water, which is also in agreement with FTIR analysis. However, the secondary structure modification in **L-WSN5-w** is small and would not alone justify such a reduction in hydrolysis yield. Another contribution can be due to the higher con- centration of lipase molecules immobilized in closed form with respect to **L-WSN5** (for the lower concentration in solution) and inhibition of the interfacial activation caused by the interaction with the support. This result confirms the key role played by the oil phase in the immo- bilization phase, even if it is present in very small amounts.

Transesterification tests were carried out for free enzyme and **L- WSN5**. The free enzyme was able to produce 600 mg of glycerol from 9.2 g of sunflower oil, corresponding to a yield of reaction equal to 56%. The yield of the transesterification reaction was in this case lower than that of the hydrolysis reaction. The possible reason is the well-known inhibitory effect of short chain alcohols such as methanol and ethanol on lipase activity [78,79]. **L-WSN5** was able to produce 1 g glycerol, corresponding to a YR (%) of 93%. In this case, the yield of trans- esterification was higher than the yield of hydrolysis. This is probably due to the different partitioning of ethanol between the surfactant/oil solution and the microenvironment of the immobilized lipase [80]. The immobilized lipase can be exposed to a lower concentration of ethanol with respect to the bulk oil phase, due to the low affinity of the hydro- phobized WSNs with polar short-chain alcohols. Moreover, the hydro- phobic WSNs are probably better dispersed in the apolar oil phase than in presence of excess water, as in the hydrolysis environment. Finally, these results confirm the hyperactivation of lipase. The results of catalytic assays for both hydrolysis and transesterification reactions are summarized in Table 3.

Operational stability tests were carried out using **L-WSN5** to assess the reusability of the supported biocatalysts. From Fig. 7b it can be seen that the catalyst maintains its activity for the hydrolysis of triglycerides up to 6th cycle. Reusability tests performed on lipase immobilized on unfunctionalized WSNs showed a gradual decrease of activity with increasing recycling time, ascribed to the leaching of immobilized lipase during successive hydrolysis reactions [18]. On the other hand, lipase immobilized on hydrophobic supports often shows optimal recycling [76]. Indeed, the higher the hydrophobicity of the surface, the stronger is the lipase-support affinity. So, desorption from a hydrophilic matrix is easier if compared to the case of a hydrophobic support [81]. In the seventh cycle, a decrease in conversion to 70% was obtained, which can be attributed to a detectable loss of catalyst after repeated recovery operations. For this reason, any further measurements were considered unreliable.

4. Conclusions

In this work, lipase was immobilized by adsorption on hydrophobic WSNs. WSNs were hydrophobized using perfluorodecyltriethoxysilane (PDTES) in different amounts. The adsorption was carried out from a micro-oily environment (water-n-hexane). **WSN1**, **WSN5** and **WSN10**, showed excellent hydrophobicity. The obtained results made these substrates suitable candidates for lipase immobilization via interfacial adsorption, allowing preferentially lipase immobilization on the support in the open conformation. The analysis of amide I band of the FTIR spectra pointed out that the native conformation of lipase was better preserved in the biocatalyst **LWSN5**. This result highlighted an impor- tant role played by n-hexane in the water/lipase solution used for lipase adsorption, favouring loading and stabilizing the native conformation. The best biocatalyst obtained (**LWSN5**) was tested in both the hydrolysis and transesterification of triglycerides and compared to free lipase. The yields of hydrolysis was 87% for supported lipase, compared to a yield of 76% for free lipase. Similarly, the transesterification yield achieved by **L-WSN5** (93%) was higher than free lipase (56%). Finally, recycling study carried out using 7 consecutive cycles demonstrated the easy recoverability of the immobilized biocatalyst system and its practical application potential.

CRediT authorship contribution statement

Giulio Pota: Investigation, Writing – review & editing. **Aurelio Bifulco:** Investigation, Validation. **Dambarudhar Parida:** Methodol- ogy, Writing – original draft. **Shanyu Zhao:** Investigation. **Daniel Rentsch:** Investigation. **Eugenio Amendola:** Investigation, Formal analysis. **Valeria Califano:** Conceptualization, Writing – original draft. **Aniello Costantini:** Project administration, Writing – review & editing.

Declaration of competing interest

The authors declare that they have no known competing financial interests or personal relationships that could have appeared to influence the work reported in this paper.

Acknowledgments

We are thankful to Mr. Mario De Angioletti from the Institute for Polymers, Composites, and Biomaterials of the National Research Council of Italy for the experimental support in performing contact angle measurements. The NMR hardware was partially granted by the Swiss National Science Foundation (SNS, grant no. 206021_150638/1)

References

[1] S. Di Iorio, A. Magno, E. Mancaruso, B.M. Vaglieco, L. Arnone, L. Dal Bello, Engine Performance and Emissions of a Small Diesel Engine Fueled with Various Diesel/ RME Blends, SAE Technical Paper, 2014.

[2] M. Sarno, M. Iuliano, Highly active and stable Fe3O4/Au nanoparticles supporting lipase catalyst for biodiesel production from waste tomato, Appl. Surf. Sci. 474 (2019) 135–146.

[3] M. Babaki, M. Yousefi, Z. Habibi, M. Mohammadi, P. Yousefi, J. Mohammadi, J. Brask, Enzymatic production of biodiesel using lipases immobilized on silica nanoparticles as highly reusable biocatalysts: effect of water, t-butanol and blue silica gel contents, Renew. Energy 91 (2016) 196–206.

[4] M. Babaki, M. Yousefi, Z. Habibi, M. Mohammadi, J. Brask, Effect of water, organic solvent and adsorbent contents on production of biodiesel fuel from canola oil catalyzed by various lipases immobilized on epoxy-functionalized silica as low cost biocatalyst, J. Mol. Catal. B Enzym. 120 (2015) 93–99.

[5] X. Liang, Synthesis of biodiesel from waste oil under mild conditions using novel acidic ionic liquid immobilization on poly divinylbenzene, Energy 63 (2013) 103–108.

[6] X. Fang, X. Zhao, W. Fang, C. Chen, N. Zheng, Self-templating synthesis of hollow mesoporous silica and their applications in catalysis and drug delivery, Nanoscale 5 (2013) 2205–2218.

[7] J.K. Poppe, R. Fernandez-Lafuente, R.C. Rodrigues, M.A.Z. Ayub, Enzymatic reactors for biodiesel synthesis: present status and future prospects, Biotechnol. Adv. 33 (2015) 511–525.

[8] S. Arana-Pen˜a, D. Carballares, A´ . Berenguer-Murcia, A.R. Alc´antara, R. C. Rodrigues, R. Fernandez-Lafuente, One pot use of combilipases for full modification of oils and fats: multifunctional and heterogeneous substrates, Catalysts 10 (2020) 605.

[9] R.C. Rodrigues, C. Ortiz, A´ . Berenguer-Murcia, R. Torres, R. Ferna´ndez-Lafuente, Modifying enzyme activity and selectivity by immobilization, Chem. Soc. Rev. 42 (2013) 6290–6307.

[10] C. Mateo, J.M. Palomo, G. Fernandez-lorente, J.M. Guisan, R. Fernandez-lafuente, Improvement of enzyme activity , stability and selectivity via immobilization techniques Improvement of enzyme activity, stability and selectivity via immobilization techniques (2007), https://doi.org/10.1016/j. enzmictec.2007.01.018.

[11] C. Garcia-Galan, A´ . Berenguer-Murcia, R. Fernandez-Lafuente, R.C. Rodrigues, Potential of different enzyme immobilization strategies to improve enzyme performance, Adv. Synth. Catal. 353 (2011) 2885–2904.

[12] D. Nourozian, Enzyme Immobilization: the State of Art in Biotechnology, 2003.

[13] E.P. Cipolatti, E.A. Manoel, R. Fernandez-Lafuente, D.M.G. Freire, Support engineering: relation between development of new supports for immobilization of lipases and their applications, Biotechnol. Res. Innov. 1 (2017) 26–34.

[14] B. Silvestri, A. Pezzella, G. Luciani, A. Costantini, F. Tescione, F. Branda, Heparin conjugated silica nanoparticle synthesis, Mater. Sci. Eng. C 32 (2012) 2037–2041.

[15] B. Zou, C. Song, X. Xu, J. Xia, S. Huo, F. Cui, Enhancing stabilities of lipase by enzyme aggregate coating immobilized onto ionic liquid modified mesoporous materials, Appl. Surf. Sci. 311 (2014) 62–67.

[16] F. Sannino, S. Ruocco, A. Marocco, S. Esposito, M. Pansini, Simazine removal from waters by adsorption on porous silicas tailored by sol–gel technique, Microporous Mesoporous Mater. 180 (2013) 178–186.

[17] G. Luciani, A. Costantini, B. Silvestri, F. Tescione, F. Branda, A. Pezzella, Synthesis, structure and bioactivity of pHEMA/SiO 2 hybrids derived through in situ sol–gel process, J. Sol. Gel Sci. Technol. 46 (2008) 166–175.

[18] F. Branda, A. Bifulco, D. Jehnichen, D. Parida, R. Pauer, J. Passaro, S. Gaan,
D. Pospiech, M. Durante, Structure and bottom-up formation mechanism of multisheet silica-based nanoparticles formed in an epoxy matrix through an in situ process, Langmuir 37 (2021) 8886–8893.

[19] A. Bifulco, F. Tescione, A. Capasso, P. Mazzei, A. Piccolo, M. Durante, M. Lavorgna, G. Malucelli, F. Branda, Effects of post cure treatment in the glass transformation range on the structure and fire behavior of in situ generated silica/epoxy hybrids, J. Sol. Gel Sci. Technol. 87 (2018) 156–169.

[20] Y. Wang, X. Du, Z. Liu, S. Shi, H. Lv, Dendritic fibrous nano-particles (DFNPs): rising stars of mesoporous materials, J. Mater. Chem. A. 7 (2019) 5111–5152.

[21] V. Venezia, F. Sannino, A. Costantini, B. Silvestri, S. Cimino, V. Califano, Mesoporous silica nanoparticles for β-glucosidase immobilization by templating with a green material: tannic acid, Microporous Mesoporous Mater. 302 (2020) 110203.

[22] D.-S. Moon, J.-K. Lee, Tunable synthesis of hierarchical mesoporous silica nanoparticles with radial wrinkle structure, Langmuir 28 (2012) 12341–12347.

[23] J. Pang, G. Zhou, R. Liu, T. Li, Esterification of oleic acid with methanol by immobilized lipase on wrinkled silica nanoparticles with highly ordered, radially oriented mesochannels, Mater. Sci. Eng. C 59 (2016) 35–42.

[24] V. Califano, A. Costantini, B. Silvestri, V. Venezia, S. Cimino, F. Sannino, The effect of pore morphology on the catalytic performance of β-glucosidase immobilized into mesoporous silica, Pure Appl. Chem. 91 (2019) 1583–1592.

[25] V. Califano, F. Sannino, A. Costantini, J. Avossa, S. Cimino, A. Aronne, Wrinkled silica nanoparticles: efficient matrix for β-glucosidase immobilization, J. Phys. Chem. C 122 (2018) 8373–8379.

[26] F. Sannino, A. Costantini, F. Ruffo, A. Aronne, V. Venezia, V. Califano, Covalent immobilization of β-glucosidase into mesoporous silica nanoparticles from anhydrous acetone enhances its catalytic performance, Nanomaterials 10 (2020) 108.
[27] M. Kalantari, M. Yu, Y. Liu, X. Huang, C. Yu, Engineering mesoporous silica microspheres as hyper-activation supports for continuous enzymatic biodiesel production, Mater. Chem. Front. 3 (2019) 1816–1822.
[28] P. Grochulski, Y. Li, J.D. Schrag, M. Cygler, Two conformational states of Candida rugosa lipase, Protein Sci. 3 (1994) 82–91.
[29] M. Cygler, J.D. Schrag, Structure and conformational flexibility of Candida rugosa lipase, Biochim. Biophys. Acta Mol. Cell Biol. Lipids 1441 (1999) 205–214.
[30] P.D. De Maria, J.M. S´anchez-Montero, J.V. Sinisterra, A.R. Alca´ntara, Understanding Candida rugosa lipases: an overview, Biotechnol. Adv. 24 (2006) 180–196.
[31] E.A. Manoel, J.C.S. Dos Santos, D.M.G. Freire, N. Rueda, R. Fernandez-Lafuente, Immobilization of lipases on hydrophobic supports involves the open form of the enzyme, Enzym. Microb. Technol. 71 (2015) 53–57.
[32] Z.D. Kne˘zevi´c, S.S. S˘iler-Marinkovi´c, L.V. Mojovi´c, Immobilized lipases as practical catalysts, Acta Period. Technol. (2004) 151–164.
[33] R. Fernandez-Lafuente, P. Armis´en, P. Sabuquillo, G. Fern´andez-Lorente, J. M. Guis´an, Immobilization of lipases by selective adsorption on hydrophobic supports, Chem. Phys. Lipids 93 (1998) 185–197.
[34] J.M. Palomo, G. Mun˜oz, G. Fern´andez-Lorente, C. Mateo, R. Ferna´ndez-Lafuente, J. M. Guis´an, Interfacial adsorption of lipases on very hydrophobic support (octadecyl–Sepabeads): immobilization, hyperactivation and stabilization of the open form of lipases, J. Mol. Catal. B Enzym. 19 (2002) 279–286.
[35] W. Zhuang, W. Gu, Q. Zhu, J. Zhu, Z. Wang, H. Niu, D. Liu, J. Wu, Y. Chen, M. Li, Surface functionalization of graphene oxide by disodium guanosine 5′- monophosphate and its excellent performance for lipase immobilization, Appl. Surf. Sci. 492 (2019) 27–36.
[36] V. Dossat, D. Combes, A. Marty, Continuous enzymatic transesterification of high oleic sunflower oil in a packed bed reactor: influence of the glycerol production, Enzym. Microb. Technol. 25 (1999) 194–200.
[37] A.B. Martins, M.F. Schein, J.L.R. Friedrich, R. Fernandez-Lafuente, M.A.Z. Ayub, R. C. Rodrigues, Ultrasound-assisted butyl acetate synthesis catalyzed by Novozym 435: enhanced activity and operational stability, Ultrason. Sonochem. 20 (2013) 1155–1160.
[38] N. Paludo, J.S. Alves, C. Altmann, M.A.Z. Ayub, R. Fernandez-Lafuente, R. C. Rodrigues, The combined use of ultrasound and molecular sieves improves the synthesis of ethyl butyrate catalyzed by immobilized Thermomyces lanuginosus lipase, Ultrason. Sonochem. 22 (2015) 89–94.
[39] R.C. Rodrigues, J.J. Virgen-Ortíz, J.C.S. Dos Santos, A´ . Berenguer-Murcia, A. R. Alcantara, O. Barbosa, C. Ortiz, R. Fernandez-Lafuente, Immobilization of lipases on hydrophobic supports: immobilization mechanism, advantages, problems, and solutions, Biotechnol. Adv. 37 (2019) 746–770.
[40] E. S´everac, O. Galy, F. Turon, C.A. Pantel, J.-S. Condoret, P. Monsan, A. Marty, Selection of CalB immobilization method to be used in continuous oil transesterification: analysis of the economical impact, Enzym. Microb. Technol. 48 (2011) 61–70.
[41] V. Califano, F. Bloisi, G. Perretta, A. Aronne, G. Ausanio, A. Costantini, L. Vicari, Frozen microemulsions for MAPLE immobilization of lipase, Molecules 22 (2017) 2153.
[42] J. Wongwatanapaiboon, W. Malilas, C. Ruangchainikom, G. Thummadetsak, S. Chulalaksananukul, A. Marty, W. Chulalaksananukul, Overexpression of Fusarium solani lipase in Pichia pastoris and its application in lipid degradation, Biotechnol. Biotechnol. Equip. 30 (2016) 885–893.
[43] Y. Lokha, S. Arana-Pen˜a, N.S. Rios, C. Mendez-Sanchez, L.R.B. Gonçalves, F. Lopez-Gallego, R. Fernandez-Lafuente, Modulating the properties of the lipase from Thermomyces lanuginosus immobilized on octyl agarose beads by altering the immobilization conditions, Enzym. Microb. Technol. 133 (2020) 109461.
[44] S. Arana-Pen˜a, N.S. Rios, D. Carballares, C. Mendez-Sanchez, Y. Lokha, L.R. B. Gonçalves, R. Fernandez-Lafuente, Effects of enzyme loading and immobilization conditions on the catalytic features of lipase from Pseudomonas fluorescens immobilized on octyl-agarose beads, Front. Bioeng. Biotechnol. 8 (2020) 36.
[45] S. Arana-Pen˜a, N.S. Rios, D. Carballares, L.R.B. Goncalves, R. Fernandez-Lafuente, Immobilization of lipases via interfacial activation on hydrophobic supports: production of biocatalysts libraries by altering the immobilization conditions, Catal. Today 362 (2021) 130–140.
[46] C. Alimentarius, Codex standard for named vegetable oils, Codex Stan 210 (1999) 1–13.
[47] H.B. Eral, J.M. Oh, Contact angle hysteresis: a review of fundamentals and applications, Colloid Polym. Sci. 291 (2013) 247–260.
[48] D.K. Owens, Some thermodynamic aspects of polymer adhesion, J. Appl. Polym. Sci. 14 (1970) 1725–1730.
[49] A. Stojanovic, S.P. Comesan˜a, D. Rentsch, M.M. Koebel, W.J. Malfait, Ambient pressure drying of silica aerogels after hydrophobization with mono-, di-and tri- functional silanes and mixtures thereof, Microporous Mesoporous Mater. 284 (2019) 289–295.
[50] V. Venezia, A. Costantini, G. Landi, A. Di Benedetto, F. Sannino, V. Califano, Immobilization of β-glucosidase over structured cordierite monoliths washcoated with wrinkled silica nanoparticles, Catalysts 10 (2020) 889.
[51] A.K. Kota, G. Kwon, A. Tuteja, The design and applications of superomniphobic surfaces, NPG Asia Mater. 6 (2014) e109–e109.
[52] D. Parida, M. Jassal, A.K. Agarwal, Functionalization of cotton by in-situ reaction of styrene in atmospheric pressure plasma zone, Plasma Chem. Plasma Process. 32 (2012) 1259–1274.
[53] S. Jiang, Q. Chen, M. Tripathy, E. Luijten, K.S. Schweizer, S. Granick, Janus particle synthesis and assembly, Adv. Mater. 22 (2010) 1060–1071.
[54] F.M. Fowkes, Attractive forces at interfaces, Ind. Eng. Chem. 56 (1964) 40–52. [55] F. Fowkes, Determination of intermolecular forces by surface-chemical techniques, in: Adhesion, ASTM International, 1964.
[56] D.K. Owens, R.C. Wendt, Estimation of the surface free energy of polymers, J. Appl. Polym. Sci. 13 (1969) 1741–1747.
[57] E.J. Chibowski, Surface free energy and wettability of silyl layers on silicon determined from contact angle hysteresis, Adv. Colloid Interface Sci. 113 (2005) 121–131.
[58] J.M. Palomo, M. Filice, O. Romero, J.M. Guisan, Improving lipase activity by immobilization and post-immobilization strategies, in: Immobil. Enzym. Cells, Springer, 2013, pp. 255–273.
[59] J. Kecht, A. Schlossbauer, T. Bein, Selective functionalization of the outer and inner surfaces in mesoporous silica nanoparticles, Chem. Mater. 20 (2008) 7207–7214.
[60] M.H. Lim, A. Stein, Comparative studies of grafting and direct syntheses of inorganic- organic hybrid mesoporous materials, Chem. Mater. 11 (1999) 3285–3295.
[61] D. Brühwiler, Postsynthetic functionalization of mesoporous silica, Nanoscale 2 (2010) 887–892.
[62] D. Parida, K.A. Salmeia, A. Sadeghpour, S. Zhao, A.K. Maurya, K.I. Assaf, E. Moreau, R. Pauer, S. Lehner, M. Jovic, Template-free

synthesis of hybrid silica nanoparticle with functionalized mesostructure for efficient methylene blue removal, Mater. Des. 201 (2021) 109494.
[63] A. Adamczyk, Y. Xu, B. Walaszek, F. Roelofs, T. Pery, K. Pelzer, K. Philippot, B. Chaudret, H.-H. Limbach, H. Breitzke, Solid state and gas phase NMR studies of immobilized catalysts and catalytic active nanoparticles, Top. Catal. 48 (2008) 75–83.
[64] H. Zaak, E.-H. Siar, J.F. Kornecki, L. Fernandez-Lopez, S.G. Pedrero, J.J. Virgen- Ortíz, R. Fernandez-Lafuente, Effect of immobilization rate and enzyme crowding on enzyme stability under different conditions. The case of lipase from Thermomyces lanuginosus immobilized on octyl agarose beads, Process Biochem. 56 (2017) 117–123.
[65] A. Natalello, D. Ami, S. Brocca, M. Lotti, S.M. Doglia, Secondary structure, conformational stability and glycosylation of a recombinant Candida rugosa lipase studied by Fourier-transform infrared spectroscopy, Biochem. J. 385 (2005) 511–517.
[66] S. Ranaldi, V. Belle, M. Woudstra, J. Rodriguez, B. Guigliarelli, J. Sturgis, F. Carriere, A. Fournel, Lid opening and unfolding in human pancreatic lipase at low pH revealed by site-directed spin labeling EPR and FTIR spectroscopy, Biochemistry 48 (2009) 630–638.
[67] Y. Yang, J. Wu, T. Xiao, Z. Tang, J. Shen, H. Li, Y. Zhou, Z. Zou, Urchin-like hierarchical CoZnAl-LDH/RGO/g-C3N4 hybrid as a Z-scheme photocatalyst for efficient and selective CO2 reduction, Appl. Catal. B Environ. 255 (2019) 117771, https://doi.org/10.1016/j.apcatb.2019.117771.
[68] J.L.R. Arrondo, A. Muga, J. Castresana, F.M. Gon˜i, Quantitative studies of the structure of proteins in solution by Fourier-transform infrared spectroscopy, Prog. Biophys. Mol. Biol. 59 (1993) 23–56.
[69] A. Aronne, G. Ausanio, F. Bloisi, R. Calabria, V. Califano, E. Fanelli, P. Massoli, L.R. M. Vicari, Structural characterization of MAPLE deposited lipase biofilm, Appl. Surf. Sci. 320 (2014) 524–530.
[70] Z. Zhou, A. Inayat, W. Schwieger, M. Hartmann, Improved activity and stability of lipase immobilized in cage-like large pore mesoporous organosilicas, Microporous Mesoporous Mater. 154 (2012) 133–141.
[71] L. Chronopoulou, G. Kamel, C. Sparago, F. Bordi, S. Lupi, M. Diociaiuti, C. Palocci, Structure–activity relationships of Candida rugosa lipase immobilized on polylactic acid nanoparticles, Soft Matter 7 (2011) 2653–2662.
[72] S. Soni, B.P. Dwivedee, U.C. Banerjee, Facile fabrication of a recyclable nanobiocatalyst: immobilization of Burkholderia cepacia lipase on carbon nanofibers for the kinetic resolution of a racemic atenolol intermediate, RSC Adv. 8 (2018) 27763–27774.
[73] S. Noinville, M. Revault, M.-H. Baron, A. Tiss, S. Yapoudjian, M. Ivanova, R. Verger, Conformational changes and orientation of Humicola lanuginosa lipase on a solid hydrophobic surface: an in situ interface Fourier transform infrared- attenuated total reflection study, Biophys. J. 82 (2002) 2709–2719.
[74] F.D. Pitt, A.M. Domingos, A.A.C. Barros, Purification of residual glycerol recovered from biodiesel production, S. Afr. J. Chem. Eng. 29 (2019) 42–51.
[75] R.C. Rodrigues, M.A.Z. Ayub, Effects of the combined use of Thermomyces lanuginosus and Rhizomucor miehei lipases for the transesterification and hydrolysis of soybean oil, Process Biochem. 46 (2011) 682–688.
[76] M. Kalantari, M. Yu, Y. Yang, E. Strounina, Z. Gu, X. Huang, J. Zhang, H. Song, C. Yu, Tailoring mesoporous-silica nanoparticles for robust immobilization of lipase and biocatalysis, Nano Res 10 (2017) 605–617.
[77] W. Jin, Y. Xu, X.-W. Yu, Preparation of lipase cross-linked enzyme aggregates in octyl-modified mesocellular foams, Int. J. Biol. Macromol. 130 (2019) 342–347.
[78] C.C. Akoh, S.-W. Chang, G.-C. Lee, J.-F. Shaw, Enzymatic approach to biodiesel production, J. Agric. Food Chem. 55 (2007) 8995–9005.
[79] L.P. Christopher, H. Kumar, V.P. Zambare, Enzymatic biodiesel: challenges and opportunities, Appl. Energy 119 (2014) 497–520.
[80] M. Zoumpanioti, H. Stamatis, A. Xenakis, Microemulsion-based organogels as matrices for lipase immobilization, Biotechnol. Adv. 28 (2010) 395–406.
[81] V.M. Balcao, M.C. Vieira, F.X. Malcata, Adsorption of protein from several commercial lipase preparations onto a hollow-fiber membrane module, Biotechnol. Prog. 12 (1996) 164–172.

Figures

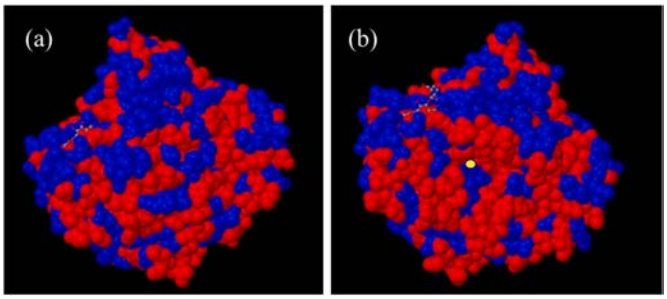

Fig. 1. Candida rugosa lipase surface structure. (a) Closed form and (b) open form. Red: hydrophobic amino acids, blue: hydrophilic amino acids, yellow: Ser 209 belonging to the catalytic triad [29] (RCSB Protein Data Bank). (For interpretation of the references to colour in this figure legend, the reader is referred to the Web version of this article.)

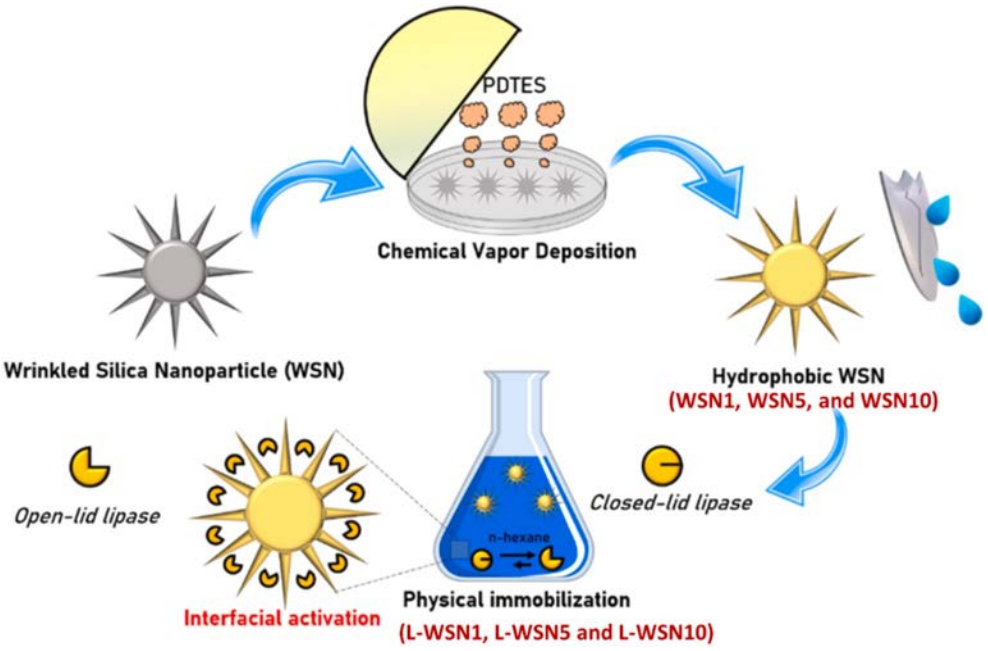

Fig. 2. Graphical sketch of the overall experimental route for production of supported biocatalysts.

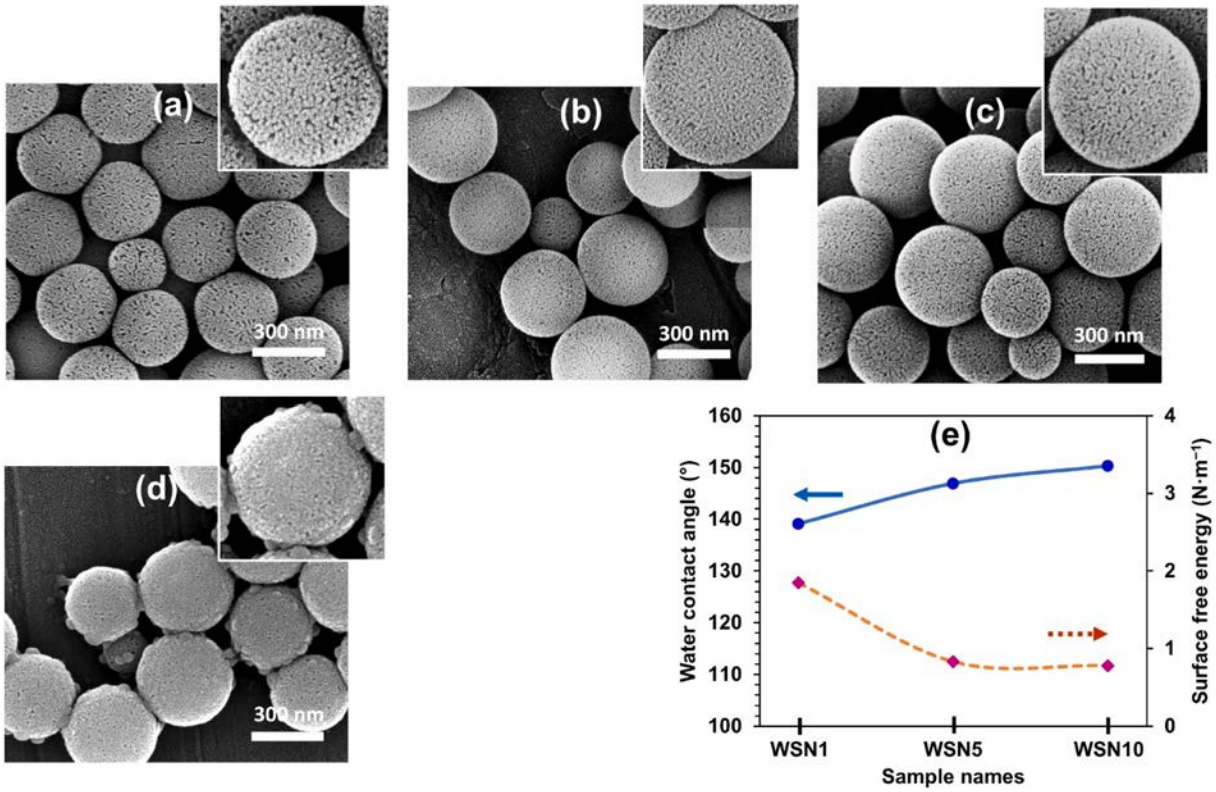

Fig. 3. SEM images of (a) **WSN**, (b) **WSN1**, (c) **WSN5**, (d) **WSN10**, and (e) figure showing the contact angle (CA) and surface free energy (SFE) of pristine and functionalized WSNs.

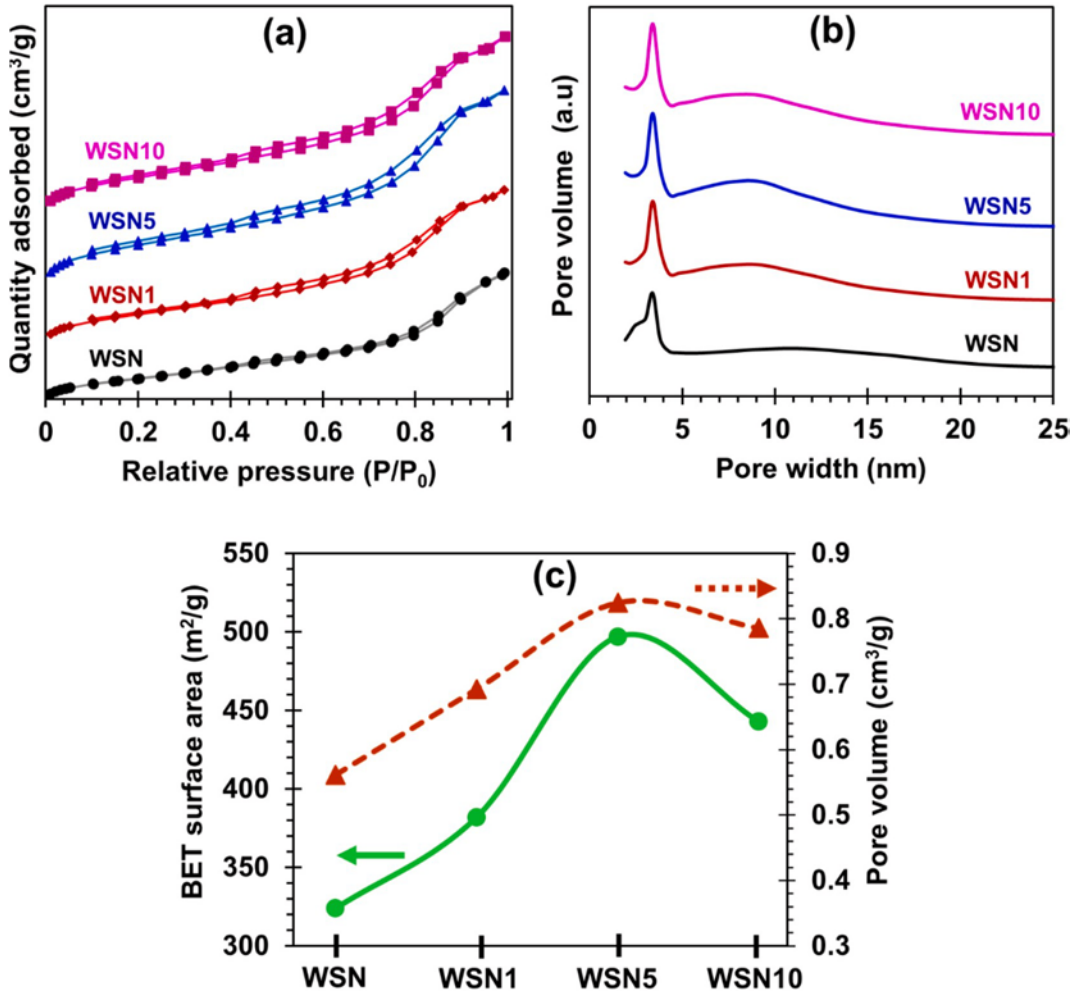

Fig. 4. (a) N_2 adsorption–desorption isotherm and the sorption of all curves starts from 0 cm^3/g at $p/p_0 = 0$. (b) pore size distribution, and (c) change in surface area and pore volume with hydrophobic functionalization of WSNs.

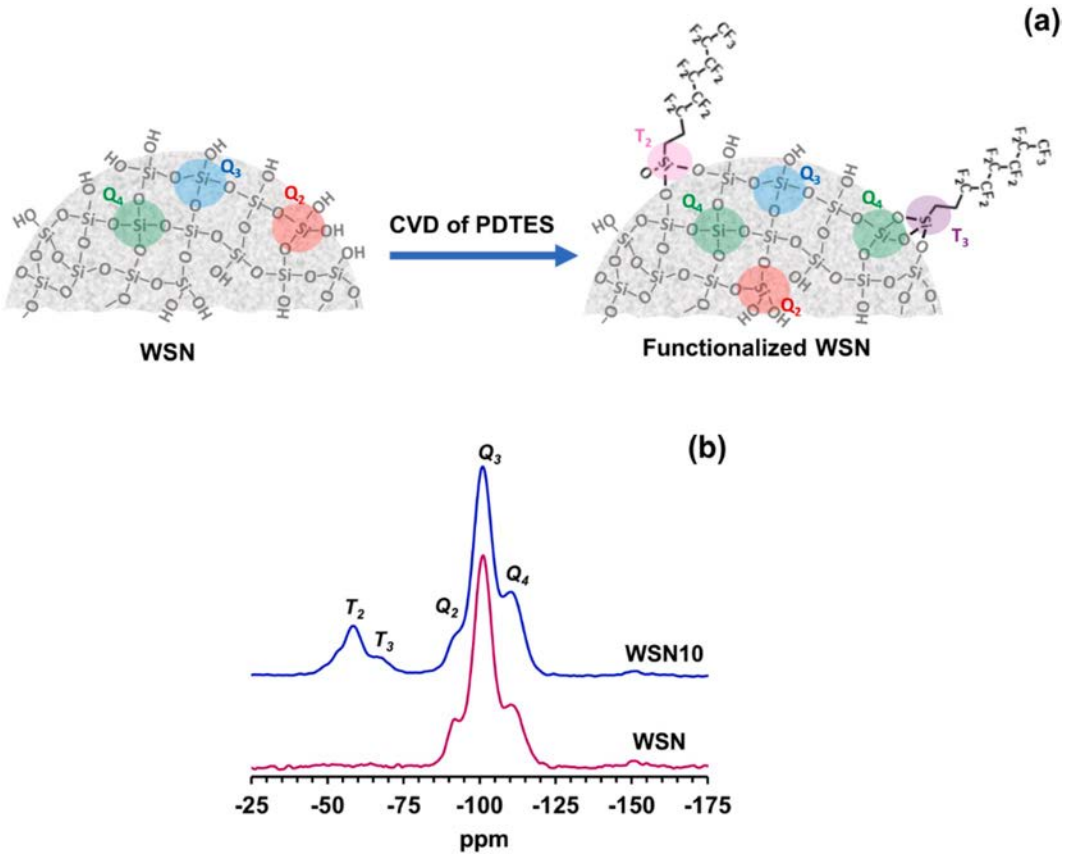

Fig. 5. (a) Simplified schematic representation showing grafting of PDTES on the WSNs during the CVD process. (b) ^{29}Si CP MAS NMR spectra of unfunctionalized **WSNs** and after hydrophobic functionalization of silica nanoparticles (**WSN10**).

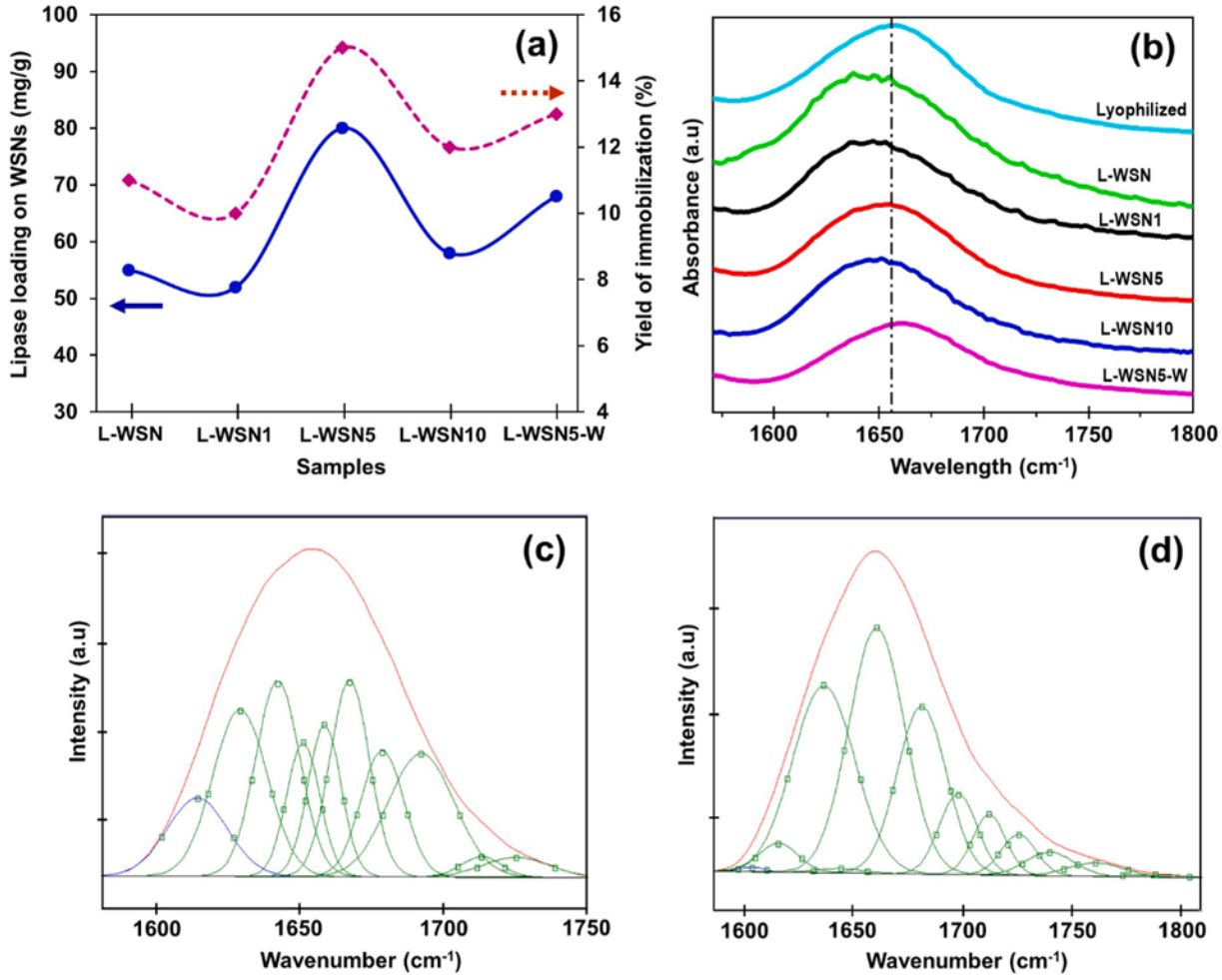

Fig. 6. (a) Lipase loading (mg/g) and yield of immobilization (%) for all the supported biocatalysts. FT-IR spectra with (b) focus on amide I region of lyophilized lipase, lipase adsorbed on **WSNs**, **WSN1-10** from water/hexane, and adsorbed on **WSN5** from water. (c) Experimental and calculated curves with best fits by Gaussian components of amide I band from **L-WSN5** and from (d) **L-WSN5-w**.

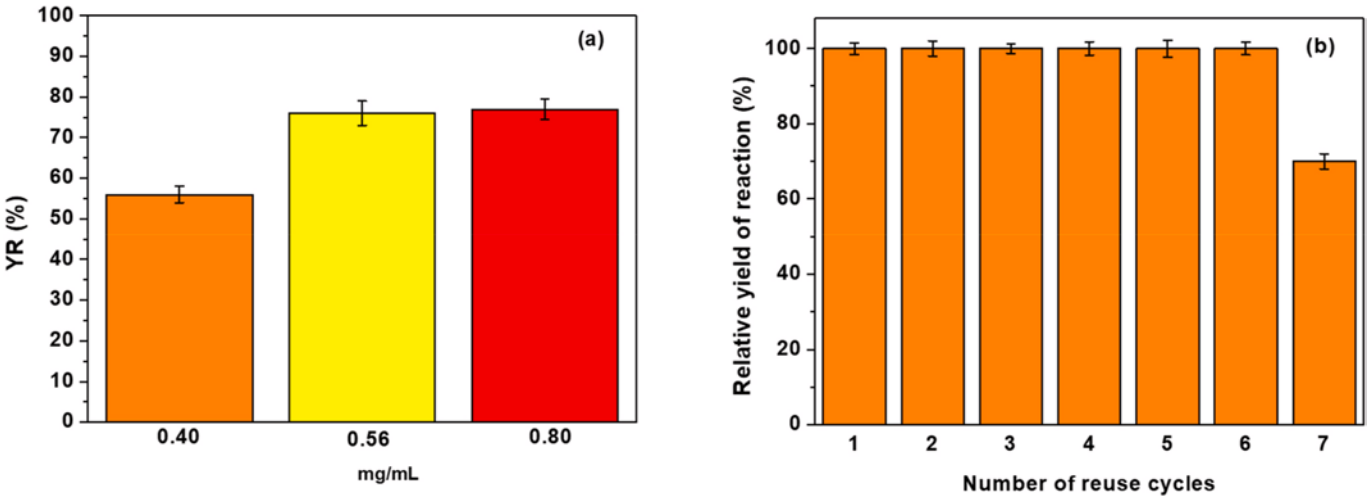

Fig. 7. (a) Yield of reaction for different enzyme concentrations. (b) The relative yield of reaction histograms over the number of cycles of reaction.

Tables

Table 1
Peak attribution of Amide I band for **L-WSN5** and **L-WSN5-w**.

Attribution β-turn content in **L-WSN5-w** also indicates a change in the secondary structure [72].

1614.1 ± 3.9	1616.1 ± 2.6	Aggregates
1629.1 ± 3.7	1628.6 ± 10.7	B-sheets
1642.4 ± 2.5	1638.5 ± 4.1	α-helices/ unordered
1651.3 ± 8.6	1649.7 ± 1.2	α-helices
1658.8 ± 4.1	1659.4 ± 9.8	α-helices
1667.7 ± 5.1	1670.6 ± 5.0	β-turns
1679.2 ± 11.9	1683.1 ± 6.7	Aggregates
1693.8 ± 13.6	1693.1 ± 2.8	β-sheets/turns

Table 2
Secondary structure elements of **L-WSN5** and **LWSN5-w**, compared to a litera- ture case * [65,73].

Secondary structure elements	L-WSN5 [%]	L-WSN5-w [%]	Literature* [%]
Aggregates	19.1	12.9	5
β-sheets	24.7	25.2	26
α-helices	25.8	19.7	33
β-turns	22.2	29.6	27
Unordered	8.0	10.0	9

Yield of reaction (YR %) for hydrolysis and transesterification reported for free lipase, **L-WSN5** and **L-WSN5-w** biocatalysts.

Sample	Hydrolysis YR [%]	Transesterification YR [%]
Free lipase	76	56
L-WSN5	87	93
L-WSN5-w	45	/